Energy Conversion and Management 327 (2025) 119554

Contents lists available at ScienceDirect

Energy Conversion and Management

journal homepage: www.elsevier.com/locate/enconman

Research paper

Multi-objective optimisation of a geothermal-liquefied natural gas combined organic Rankine cycle system under different distribution pressures

Han Zhang, Giovanna Cavazzini, Giacomo Zanetti, Alberto Benato *

Department of Industrial Engineering, University of Padova, Via Venezia 1, Padova, 35131, Italy

ARTICLE INFO

Keywords:
Geothermal energy
Organic Rankine cycle
Liquefied natural gas
Working fluid optimisation
Configuration optimisation

ABSTRACT

Multi-objective optimisation is drawing more and more attention in the organic Rankine cycle research field due to its comprehensiveness in demonstrating optimum results from multiple perspectives. For this reason, a comparative two-objective optimisation is performed on a combined organic Rankine cycle system liquefied with geothermal among three typical distribution pressures: 1 MPa, 4 MPa and 7 MPa. Eight operational parameters, 11 working fluids, and 16 possible configurations are included during optimisation. The optimisation result is divided and analysed on the basis of the thermodynamic weight (W_1). The results reveal that the recuperative organic Rankine cycle configuration is preferred when W_1 is higher, while the basic organic Rankine cycle configuration is preferred when W_1 is lower. Two typical cases are further analysed in detail: the balanced case ($W_1 = 0.5$) and the maximum case ($W_1 = 1$). The system is able to yield the maximum energy efficiency of 32.78% with the working fluid Propane under the maximum case with a distribution pressure of 1 MPa. Compared to the maximum case, the balanced case is capable of achieving considerable economic benefits while incurring minimal thermodynamic losses. When the distribution pressure is 7 MPa, the balanced case can achieve as much as 82.94% of the energy efficiency compared to the maximum case, requiring only 44.17% of the electricity production cost.

1. Introduction

As world energy demands continue to increase, there is an increasingly urgent need for renewable energy. The development of renewable energy sources such as solar, wind, and geothermal energy is progressing rapidly. Among these renewable energy sources, geothermal energy stands out because it can provide a consistent energy source regardless of weather conditions, compared to other intermittent renewable energy sources such as solar and wind. For low-grade heat sources, such as geothermal energy, the conventional water-based Rankine cycle faces challenges in recovery. Organic Rankine cycles (ORCs) are considered one of the most effective methods for harnessing low-grade heat sources [1].

Regarding the ORC configuration, the basic ORC configuration which includes an evaporator, a turbine, a generator, a condenser, and a pump, is the simplest one. Starting from this configuration, by adding an internal heat exchanger (IHX), the heat of the turbine discharge flow can be re-utilised to preheat the compressed working fluid before entering the evaporator. Saleh et al. [2] reveal that the use of an IHX improves thermal efficiency, particularly for high-boiling substances with overhanging saturated vapour lines in subcritical processes. Hung et al. [3] highlight that the incorporation of an IHX reduces irreversibility and improves efficiency. However, Li et al. [4] argue that under certain thermal conditions, the IHX does not increase net output power and incurs additional equipment costs. Due to the varying working conditions between different studies, the results of these investigations cannot be directly compared. Therefore, it is necessary to include different configurations in the optimisation process, as highlighted by Pezzuolo et al. [5] and Redjeb et al. [6]. There are also other configurations, such as the trilateral flash cycle, the Kalina cycle, and the partial evaporation cycle but, all of them, are characterised by high complexity and costs. Note that the expansion process within the two-phase region can lead to the formation of wet steam, which contains liquid droplets. These droplets can impinge on turbine blades, thereby affecting their lifespan and increasing maintenance costs. Hence, the trilateral cycle and the partial evaporation cycle are not commonly applied in ORC and have not been taken into account in this study, as well as both the ORC environmental impact and its machines design (see e.g. Refs. [7–9]).

Regarding the cold source of an ORC, water is frequently used as a cooling source in power generation systems due to its convenience [10]. However, minor temperature differences relative to the heat source

* Corresponding author.
E-mail address: alberto.benato@unipd.it (A. Benato).

https://doi.org/10.1016/j.enconman.2025.119554
Received 14 October 2024; Received in revised form 19 January 2025; Accepted 21 January 2025
Available online 4 February 2025

Nomenclature

Abbreviations

AUX	Auxiliary heat exchanger
DEC	Direct expansion cycle
DNI	Direct normal irradiance
IHX	Internal heat exchange
LNG	Liquefied natural gas
$NBPT$	Normal boiling point temperature
NG	Natural gas
ORC	Organic Rankine cycle
$PPTD$	Pinch-point temperature difference
PSO	Particle swarm optimisation
PTC	Parabolic-trough collector
$TOPSIS$	Technique for Order Preference by Similarity to Ideal Situation

Symbols

ΔT	Temperature difference [K]
η	Efficiency [%]
τ	Time interval [h]
A	Heat transfer area [m^2]
c	Specific heat capacity [J kg^{-1} K^{-1}]
G	Irradiation [W m^{-2}]
h	Specific enthalpy [J kg^{-1}]
M	Mass flow rate [kg s^{-1}]
P	Power [W]
Q	Heat [W]
q	Quality [–]
S	Entropy [J K^{-1}]
T	Temperature [K]
U	Overall Heat Transfer Coefficient [kW m^{-2} K^{-1}]

Subscripts

amb	Ambient
b	Beam
c	Critical
cf	Cold fluid
col	Solar collector
con	Condenser
$cond$	Condensation
dis	Distribution
eva	Evaporator
$evap$	Evaporation
hf	Hot fluid
hs	Heat source
HX	Heat exchanger
i	State i
in	In, inlet
iso	Isotropy
out	Out, outlet
pin	Pinch-point
pri	Primary fluid
pu	Pump
sec	Secondary fluid
sol	Solar
sub	Subheat
sup	Superheat
sys	System
tit	Turbine inlet temperature
tur	Turbine
u	Usable
wf	Working fluid

lead to a low efficiency [11]. Using a low-temperature cold source, such as liquid natural gas (LNG), can further enhance the efficiency. In recent years, research on ORC systems that use LNG has focused mainly on optimising system configurations and selecting suitable working fluids. Zhang et al. [12] examined a hybrid steam Rankine cycle (SRC) and ORC system designed for cold climates, determining that ammonia and R600 are the most effective for achieving significant increases in net power, with results influenced by the temperature of the condenser outlet. He et al. [13] introduced a new LNG cold energy cascade utilisation system that integrates cryogenic energy storage, organic Rankine cycles, and direct cooling, resulting in a 22.48% increase in net power and a 5.17% improvement in exergetic efficiency relative to a baseline system, underscoring its scalability for large-scale cryogenic storage. Domingues et al. [14] proposed an innovative LNG regasification and power generation system using a two-stage cascade Rankine cycle with ternary mixtures as working fluids and seawater as heat source, achieving thermal and exergy efficiencies of 23.7% and 79.18%, respectively. Choi et al. [15] optimised a LNG regasification ORC under spatial constraints, emphasising the importance of heat duty and conductance allocation, and concluded that maximising the evaporator heat exchanger size ensures superior system performance for a given total conductance. Zhang et al. [16] propose a combined system using LNG exergy that demonstrates higher net power output and lower investment costs compared to separate systems. Wei et al. [17] highlight that maximising the utilisation of LNG exhaust heat significantly enhances the net power and efficiency of the ORC system. However, although these studies investigated the ORC-LNG system from various perspectives, they only examined LNG at a single distribution pressure. It should be noted that the LNG distribution pressure, which is correlated with its application, can range widely from 0.6 to 8.5 MPa [18]. Given these significant disparities in distribution pressures in different applications, such variations should also be considered.

For the combined ORC-LNG system, optimisation generally serves as an important approach to identify the ideal operational parameters, working fluids, and system configurations for an ORC system. In the literature, there are several works dealing with combined ORC-LNG system optimisation. Sun et al. [19] performed optimisations of the two-stage Rankine cycles under varying heat source temperatures and natural gas (NG) distribution pressures. The results indicated that the two-condensation Rankine cycle achieved a maximum efficiency of 30.54% at a heat source temperature of 200 °C and a distribution pressure of NG of 3 MPa, using ammonia as the working fluid. Yari et al. [20] conducted an optimisation comparative study among six different geothermal cycles to evaluate their performance and efficiency. The highest first law efficiency of 15.35% was achieved by the binary cycle with the regenerative ORC with an internal heat exchanger, using R123 as the working fluid. Although the above studies have included a comparison of various combined ORC configurations, optimisation under different configurations is conducted separately and compared afterwards. Such a method will be extremely time-consuming when system configuration becomes more complex. In addition, there are studies that have investigated the combined geothermal-LNG ORC system. Mosaffa et al. [21] conducted a comparison study between four different combined geothermal-LNG cycles. The study finds that the regenerative system has the highest energy efficiency, while the system with an internal heat exchanger has the highest exergy efficiency. The

simple system is the most cost-effective. Ghaebi et al. [22] proposed a new trigeneration system that integrates the generation of cooling, heating and electricity, using geothermal energy as a heat source and LNG as a heat sink. Emadi et al. [23] proposed a geothermal-LNG ORC energy system for power, cooling and hydrogen production, achieving 43% exergy efficiency, 10.69 MW net power, 6.09 MW cooling and 204.77 kg h^{-1} of hydrogen production. Parikhani et al. [24] proposed a new geothermal-based multigeneration system, using LNG for cold energy recovery to simultaneously produce cooling, heating, power and hydrogen. The best efficiencies of the system are found to be 62.74% for thermal energy, 33.82% for exergy, and the total cost is 125.4 $ GJ^{-1}. Further testing shows that energy efficiency can be improved by adjusting certain parameters, such as the vapour generator pressure and evaporator temperature, or lowering others, such as the mass extraction ratio and the geothermal inlet temperature. However, although up to nine optimisation parameters were included during optimisation, no comparative study was conducted with different ORC combined configurations.

In terms of the number of optimisation goals, single-objective optimisation has been widely used to optimise the ORC system's performance. The goal is often maximisation of the net power output of the ORC cycle [25,26], the thermal efficiency [27–29], or the exergy efficiency [19,30,31]. However, in many cases, ORC systems have multiple conflicting metrics, such as maximising power output and minimising total equipment costs, and they frequently exhibit a significant interplay in practical scenarios. In such a case, the single-objective optimisation technique cannot provide an optimum solution that satisfies all the objectives. Hence, there are fewer studies on the combined geothermal and LNG systems using the two-objective optimisation method compared to the single-objective optimisation study. Moreover, only a few operational parameters are included during optimisation. Table 1 enumerates the operational optimisation parameters in research papers that focus on ORC using LNG as a cold source. Owing to its complexity, the combined ORC-LNG system encompasses a total of 8 parameters. Nevertheless, the majority of studies only included a subset of these during optimisation, leading to suboptimal accuracy. Moreover, most of the literature only considers a single NG distribution pressure. Since the optimisation results are closely related to the NG distribution pressure, it is necessary to perform an experience under different NG distribution pressures.

To bridge the aforementioned gaps, this study conducted a comparative two-objective optimisation study on a combined geothermal-LNG ORC under three typical distribution pressures: 1 MPa, 4 MPa, and 7 MPa. The study aims to (1) determine and compare the optimal operational parameters, working fluids and configurations of the system under each NG distribution pressure. (2) Speed up the total time cost by including different configurations within each optimisation process. In the optimisation, both thermal and economic metrics are taken into account. (3) Investigate the impact of weight variation on the optimal solution. Eight critical operational parameters are incorporated as the optimisation variables. In addition, during the optimisation process, 11 commonly used working fluids screened and up to 16 different combined ORC configurations are included. To the authors' understanding, there has rarely been a multi-objective study with such a multitude of optimisation parameters and configurations. This research integrates practical considerations of three typical NG distribution pressures and different weights into the ORC design phase, offering an expansion of available options and an improvement in solution reliability for decision makers.

2. Methods

The studied case layouts are presented in Section 2.1, while the details of the mathematical model are provided in Section 2.2. Section 2.3 provides information on working fluid candidates. The optimisation method and the sensitivity analysis of operational parameters are described in Sections 2.4 and 2.5, respectively.

2.1. Study case description

The geothermal-LNG combined ORC system study case includes 3 parts, the geothermal heat source, the ORC system, and the DEC system. Fig. 1 provides (a) the schematic diagram and (b) the T-s diagram of the study case. The essential ORC comprises four primary parts: a pump, a turbine, an evaporator, and a condenser. Initially, the working fluid undergoes pressurisation in the pump and then gathers thermal energy from the geothermal water in the evaporator. Once heated and pressurised, the working fluid proceeds to the turbine for expansion. Subsequently, the working fluid undergoes condensation within the condenser, returning to a liquid state in preparation for the next circulation. By adding an optional additional component Internal heat exchanger (IHX), the basic ORC can be converted to the recuperative ORC. The IHE component enables the working fluid that leaves the pump to take advantage of the remaining heat of the working fluid after expansion.

In DEC, LNG is first pressurised in the pump before being sent to the condenser to absorb heat from the working fluid. Then, NG will be heated by geothermal water in the auxiliary heat exchangers (AUX) before being expanded to the distribution pressure in the turbine. After that, the heated NG undergoes expansion to match the turbine's distribution pressure. Geothermal brine is extracted from the production well, first used to heat the ORC working fluid, then used to heat supplemental LNG, and finally returned to the reinjection well.

The implementation of the mathematical model is in MATLAB environment. Data on working fluids are extracted from the REFPROP 9.1 database, which serves as a reference for the thermodynamic and transport properties of fluids, developed by the National Institute of Standards and Technology (NIST). The operational assumptions are as follows.

- The system is deemed to be in a stable state.
- The heat exchangers and the tubes have negligible pressure drops and heat losses.
- LNG is assumed to be pure methane.

The foundational system operating parameters are comprehensively detailed in Table 2.

2.2. Mathematical model

In this section, the mathematical models employed to analyse the system are presented. The models are divided into two parts: thermodynamic and economic, which are detailed in Section 2.2.1 and in Section 2.2.2, respectively.

2.2.1. Thermodynamic model

As listed in Table 3, the conservation equations for mass and energy form the cornerstone of the development of thermodynamic models. The differences between actual processes and ideal isentropic processes are adjusted by the pump and turbine isentropic efficiencies. There are two kinds of heat exchanger model, namely the basic model (for IHX, AUX1, and AUX2) and the pinch point model (for EVA and CON). For heat exchangers without phase change, the basic model is applied because it complies only with the law of energy conservation. For phase-changed heat exchangers, the pinch-point model is adopted.

In terms of the thermodynamic optimisation objective, The energy efficiency is calculated by:

$$\eta_{en} = \frac{P_{sys}}{Q_G} \tag{1}$$

where P_{sys} is the system net work output and Q_G is the input energy of the geothermal brine:

$$P_{sys} = P_{tur,RC} + P_{tur,NG} - (P_{pu,RC} + P_{pu,NG} + P_{pu,hs}) \tag{2}$$

$$Q_G = M_{hs} \cdot \left(h_{hs,in} - h_{hs,out}\right) \tag{3}$$

Table 1
Comparison of studies on combined ORC-LNG system with the present study.

Reference	T_{evap}	T_{cond}	$T_{wf,tit}$	$T_{NG,tit}$	$PPTD_{eva}$	$PPTD_{con}$	P_{LNG}	ε	P_{dis}(MPa)
Han et al. [32]	✓	✓	✓	×	×	×	×	×	3
Badami et al. [33]	✓	✓	×	×	✓	✓	✓	×	7
Ferreira et al. [34]	✓	✓	✓	✓	×	×	✓	×	8.2
Emadi et al. [18]	✓	×	×	×	✓	×	✓	×	3
Mehrenjani et al. [35]	×	✓	×	×	×	✓	✓	×	0.3
Sadreddini et al. [36]	✓	✓	✓	×	×	×	×	×	4
Pan et al. [37]	✓	×	×	×	×	×	✓	×	0.8
Sun et al. [38]	✓	✓	✓	×	×	×	✓	✓	3/8
This work	✓	✓	✓	✓	✓	✓	✓	✓	1/4/7

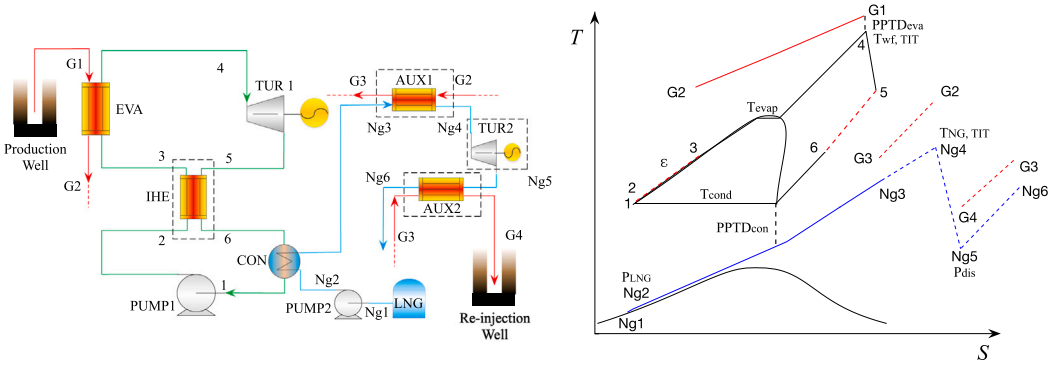

Fig. 1. The schematic diagrams and T-s diagrams of the studied system.

Table 2
The basic working conditions of the system.

Term	Parameter	Value	Unit
Geothermal brine	Inlet temperature	165	°C
	Outlet temperature limit	75	°C
LNG	Storage temperature	−162	°C
	Storage pressure	0.1	MPa
	Distribution temperature	25	°C
	Distribution pressure	1/4/7	MPa
Device [21]	Pump isentropic efficiency	90	%
	Turbine isentropic efficiency	85	%
Environment	Environmental temperature	25	°C
	Environmental pressure	0.1	MPa
Overall heat transfer coefficient [21]	Evaporator	0.85	kW m^{-2} K^{-1}
	Condenser	0.25	kW m^{-2} K^{-1}
	Internal heat exchangers	0.3	kW m^{-2} K^{-1}
	Auxiliary heat exchangers	0.2	kW m^{-2} K^{-1}

Table 3
Thermodynamic models of the main devices.

Components	Equations
Pump	$h_{pu,out} = h_{pu,in} + \frac{(h_{pu,iso} - h_{pu,in})}{\eta_{pu}}$, $P_{pu} = M_{pu}(h_{pu,out} - h_{pu,in})$
Turbine	$h_{tur,out} = h_{tur,in} - (h_{tur,in} - h_{tur,iso})\eta_{tur}$, $P_{tur} = M_{pu}(h_{tur,in} - h_{tur,out})$
Evaporator	$T_{hs,pin} = T_{wf,eva} + \Delta T_{pin,eva}$, $M_{sec} = \frac{M_{wf}(h_{wf,out} - h_{wf,eva})}{(h_{hs,in} - h_{hs,pin})}$
Condenser	$T_{cf,out} = T_{hf,in} - \Delta T_{pin,con}$, $M_{hf} = \frac{M_{cf}(h_{cf,out} - h_{cf,in})}{(h_{hf,in} - h_{hf,out})}$
AUX	$M_{hf}(h_{hf,in} - h_{hf,out}) = M_{cf}(h_{cf,out} - h_{cf,in})$
IHX	$\varepsilon = \frac{h_{cf,out} - h_{cf,in}}{h_{hf,in} - h_{cf,in}}$

2.2.2. Economic model

In terms of the thermodynamic optimisation objective, Electricity production cost (EPC) is a commonly used index to access the component's cost in an ORC system. Investment costs for an ORC system are divided among the heat exchanger, pump, and turbine. Turton [39] outline the fundamental purchasing costs, denoted as C_p, for each of these components, which are calculated using Eq. (4) (see Table 4).

Table 4
Exergy destruction rates of the main devices.

Components	Equations
Pump	$I_{pu} = P_{pu} - (E_{out} - E_{in})$
Turbine	$I_{tur} = E_{in} - E_{out} - P_{tur}$
Heat exchanger	$I_{HX} = M_{hf}(E_{hf,in} - E_{hf,out}) - M_{cf}(E_{cf,out} - E_{cf,in})$

Regarding the heat exchanger, pump and turbine, the parameter Y represents the heat exchange area, input work, and output work, respectively. Empirical coefficients $K1$, $K2$, and $K3$ are enumerated in Table 5.

$$\log C_p = K_1 + K_2 \cdot \log Y + K_3 \cdot (\log Y)^2 \tag{4}$$

The output work of the turbine or the input work of the pump is determined by the aforementioned thermodynamic models. The table referenced as Table 2 displays the heat transfer coefficients for various

Table 5
Cost parameters of each component in the system.

Component	Heat exchanger	Pump	Turbine
K_1	4.3247	3.3892	2.7051
K_2	−0.3030	0.0536	1.4398
K_2	0.1634	0.1538	−0.1776
C_1	0.03881	−0.3935	/
C_2	−0.11272	0.3957	/
C_3	0.08183	0.002626	/
B_1	1.63	1.89	/
B_2	1.66	1.35	/
F_M	1.75	2.30	/
F_{BM}	/	/	3.50

components, and the calculation of the heat exchange area is as follows:

$$A = \frac{Q_{HX}}{U \cdot \Delta T_m} \tag{5}$$

where the log mean temperature difference can be calculated by:

$$\Delta T_m = \frac{\Delta T_{max} - \Delta T_{min}}{\ln\left(\frac{\Delta T_{max}}{\Delta T_{min}}\right)} \tag{6}$$

The base cost C_P should be adjusted based on each particular component. The modified investment cost C_{BM} is determined by Eq. (7). The turbine's F_{BM} values are listed in Table 5, whereas the corresponding values for other components can be derived from Eq. (8).

$$C_{BM} = C_P \cdot F_{BM} \tag{7}$$

where F_M, denoting the material correction constant, is enumerated in Table 5, while F_p, the pressure correction coefficient, is calculated using Eq. (9).

$$F_{BM} = B_1 + B_2 \cdot F_M \cdot F_P \tag{8}$$

$$\log F_p = C_1 + C_2 \cdot \log P + C_3 \cdot (\log P)^2 \tag{9}$$

where B_1, B_2, C_1, C_2, C_3 are coefficients listed in Table 5.

The monetary statistic is presented in US dollars. Taking inflation into account, the adjusted investment cost C_{tot} is derived using Eq. (10), based on the chemical engineering plant cost index ($CEPCI$).

$$C_{tot} = \left(\sum C_{BM}\right)_{1996} \cdot \mathrm{CEPCI}_{2016}/\mathrm{CEPCI}_{1996} \tag{10}$$

where CEPCI_{1996} is 382 and CEPCI_{2016} is 542.

Furthermore, considering a 5% annualised interest rate and a 20-year lifespan for the device, the capital recovery factor (CRF) is derived in Eq. (11).

$$\mathrm{CRF} = \frac{i \cdot (1+i)^n}{(1+i)^n - 1} \tag{11}$$

Finally, the EPC for the entire system is determined using Eq. (12). The operating and maintenance costs (COM) represent 1.5% of the total capital investment in the system, and the annual operating duration of the system is 7000 h.

$$\mathrm{EPC} = \frac{\mathrm{CRF} \cdot C_{tot} + \mathrm{COM}}{T_{op} \cdot W_{net}} \tag{12}$$

2.3. Working fluid selection

The performance of the system is largely determined by the working fluids used. The appropriate working fluid ought to be eco-friendly. Consequently, the desired working fluid should be non-(or low)toxic, combined with zero ozone depletion potential (ODP) and a global warming potential (GWP) of less than 100. Furthermore, to prevent the ingress of air into the system due to condensation occurring beneath ambient pressure, the fluid's normal boiling point temperature (NBPT) is restricted to be below 25 °C. Based on the aforementioned criteria, ten common substances have been chosen as the working fluids, with their physical properties detailed in Table 6.

2.4. Optimisation method

There are in total eight operational parameters, 11 working fluids and 16 possible configurations to optimise as shown in Fig. 2. Traditional heuristic optimisation methods necessitate individual optimisation for each configuration and working fluid combination, which is highly time-consuming, especially for multi-objective optimisation. In this paper, the OSO method is employed, where all configurations are included within each optimisation by dynamically adding components based on the key parameters, significantly reducing the number of optimisations required. An innovative strategy is used to refine the configuration settings in each particle with each iteration by adding optional components: IHX, AUX1, TUR2, and AUX2. In the ORC cycle, the configuration can change from the basic ORC configuration to the recuperative ORC configuration by adding an IHX component. This transformation is linked to the optimisation of the effectiveness parameter, which determines how much heat is transferred in the IHX. In the DEC cycle, natural gas is heated in AUX1, an auxiliary heat exchanger, when its temperature is below the turbine inlet temperature. Subsequently, it experiences expansion in the TUR2 turbine if the distribution pressure exceeds the natural gas distribution pressure. Finally, AUX2, another auxiliary heat exchanger, heats the natural gas if its temperature falls short of the distribution temperature requirement. The OSO method employed has been described in detail in Ref. [40]. Hence, other details such as the particle update method and global leader selection have been omitted for the conciseness of this paper. The computational time for the combined ORC system at each distribution pressure is approximately 5 h.

There are several decision-making approaches in multi-objective optimisation, including TOPSIS, LINMAP, and Shannon Entropy. Compared to LINMAP, TOPSIS takes into account both the best and the worst feasible points and is more straightforward to implement than Shannon Entropy. Therefore, TOPSIS is used to select the final solution on the Pareto frontier. In the TOPSIS method, a weight is assigned to each objective, reflecting its relative importance [41]. For the two-objective optimisation in this study, the thermodynamic and economic weights are complementary, with the sum of the thermodynamic weight (energy efficiency) and the economic weight (EPC) equalling 1. Hence, only thermodynamic criteria are considered when the thermodynamic weight is set to 1, and economic criteria are ignored. Conversely, when the thermodynamic weight is set to 0, thermodynamic criteria are ignored and only economic criteria are considered. Moreover, thermodynamic and economic performance are treated equally when the thermodynamic weight is set to 0.5.

2.5. Sensitivity analysis

Eight operational parameters including evaporation and condensation temperatures, the effectiveness of the internal heat exchanger, the pinch-point temperature differences of the evaporator and condenser, the working fluid turbine inlet temperature, the NG turbine inlet temperature, and the LNG regasification pressure have been included as variables in the optimisation. The limits and constraints of each optimisation variable for the combined geothermal-LNG ORC system are listed in Table 7.

A sensitivity analysis is conducted to assess their influences on the thermodynamic metric energy efficiency and the economic metric EPC. Table 8 lists the typical values of the parameters studied and their variation ranges (20% around the typical value). The effects of these parameters on the thermodynamic energy efficiency metric and the economic energy consumption metric of the system are shown in Fig. 3(a) and (b), respectively. The analysis reveals that, across the studied parameter range, a higher condensation temperature, working fluid turbine inlet temperature, and LNG regasification pressure result in improved energy efficiency, while the EPC shows different trends. Specifically, the EPC reduces for the condensation temperature,

Table 6
The physical properties of the studied working fluid.

Name	Triple point temperature (°C)	Normal boiling temperature (°C)	Critical temperature (°C)	Critical pressure (MPa)	ODP	GWP
Ammonia	−77.655	−33.33	132.25	11.33	0	3.3
Butane	−138.255	−0.49	151.975	3.80	0	4
Ethane	−182.782	−88.58	32.172	4.87	0	5.5
Ethylene	−169.164	−103.77	9.2	5.04	0	4
1butene	−140.75	−7.00	144.94	4.01	0	2
Isobutane	−159.42	−11.75	134.66	3.64	0	3
Propane	−187.625	−42.11	96.74	4.25	0	5
Propylene	−185.197	−47.62	91.061	4.56	0	20
R1234ze	−104.53	−18.97	109.363	3.63	0	6
R1234yf	−53.15	−29.49	94.7	3.38	0	4
R161	−143.15	−37.55	102.1	5.01	0	4

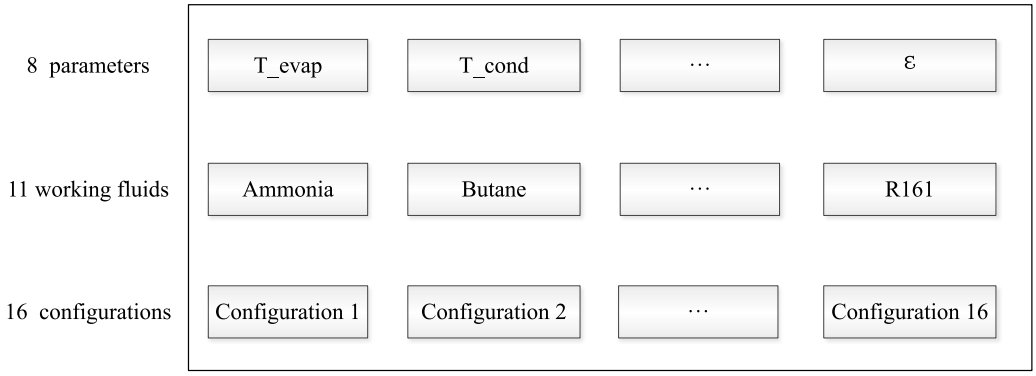

Fig. 2. The operational parameters, working fluids and configurations for optimisation.

Table 7
Boundaries and constraints of the optimisation parameters.

Term	Lower bound	Upper bound	Constrains
T_{evap}, T_{cond}	NBPT	Min $(0.99 * T_c, T_{wf,tit})$	$T_{evap} > T_{cond}$, $T_{evap} < T_{hs,in}$
$T_{wf,tit}$	NBPT	$T_{hs,in} - 5$ °C	$T_{wf,tit} > T_{evap}$
$T_{NG,tit}$	NBPT	Max $(T_6 - 5$ °C, $T_{G2O} - 5$ °C)	$T_{NG,tit} \geq T_{Ng2}$
P_{LNG}	Distribution pressure	15 MPa	–
PPTD	5 °C	–	–
Effectiveness	0	1	$T_6 > T_2 + 5$ °C

Table 8
The typical condition for sensitivity analysis.

Parameters	Unit	Typical value	Lower bound	Upper bound
Heat source temperature	°C	165	–	–
NG distribution pressure	MPa	8	–	–
Working fluid	–	Butane	–	–
Evaporation temperature	°C	70	56	84
Condensation temperature	°C	−20	−16	−24
LNG regasification pressure	MPa	8	6.4	9.6
Working fluid turbine inlet temperature	°C	95	76	114
NG turbine inlet temperature	°C	30	24	36
Evaporator PPTD	°C	60	48	72
Condenser PPTD	°C	20	16	24
Effectiveness	–	0.1	0.08	0.12

increases for the inlet temperature of the working fluid turbine, and first increases and then decreases for the regasification pressure of LNG. Energy efficiency exhibits an initial increase followed by a decline as the evaporation temperature increases, with the maximum efficiency occurring in the middle. A similar but less significant trend is shown when the inlet temperature of the NG turbine increases. As the PPTD and effectiveness of the condenser increase, both energy efficiency and EPC decrease. However, for the evaporator PPTD, energy efficiency decreases whereas EPC increases.

3. Results and discussion

Two-objective optimisations are performed for the combined geothermal-LNG ORC system under three typical natural gas distribution pressures: 1 MPa, 4 MPa, and 7 MPa for comparison.

3.1. Optimisation results

The result obtained from the two-objective optimisation is presented and the results are further analysed in terms of effectiveness and working fluid.

3.1.1. Optimum objective

The optimisation results under three typical distribution pressures are aggregated and displayed in Fig. 4(a). The optimised solutions constitute the Pareto frontier and the different symbols denote different distribution pressures. The ideal point at each distribution pressure is marked with a red circle. Under each distribution pressure, energy efficiency is positively correlated with EPC, with an increase in energy efficiency resulting in a corresponding rise in EPC. However, its extent varies in relation to the distribution pressure. Specifically, as the distribution pressure decreases, the degree to which the EPC increases with energy efficiency decreases progressively, and the system is capable of achieving a higher maximal energy efficiency while simultaneously achieving a relatively lower minimum EPC. In other words, with equiv-

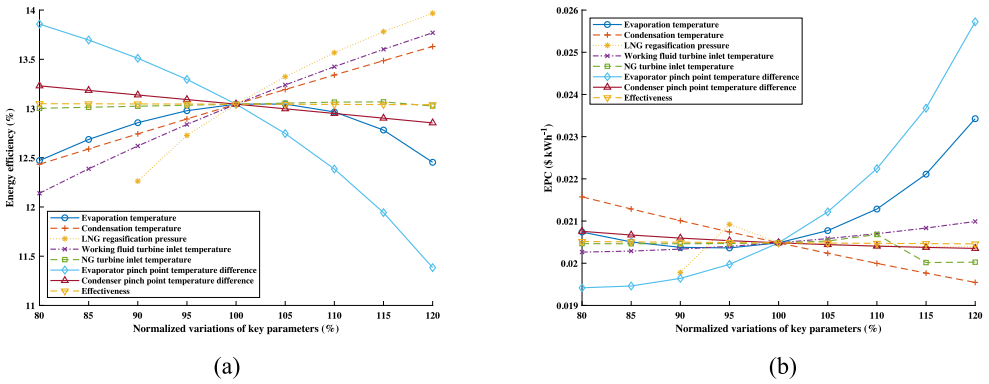

Fig. 3. The effects of key parameters on the (a) Energy efficiency; (b) EPC.

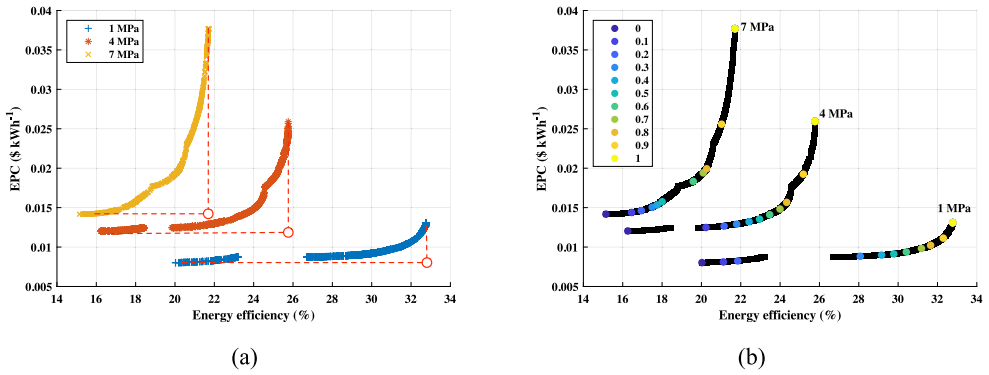

Fig. 4. (a) The optimum results under three distribution pressures 1 MPa, 4 MPa and 7 MPa; (b) Different decision optimum solutions based on the thermodynamic weights from 0 to 1 under three distribution pressures 1 MPa, 4 MPa and 7 MPa.

alent levels of energy efficiency, a lower distribution pressure yields a reduced EPC, which indicates superior economic performance.

Moreover, the results are divided on the basis of the thermodynamic weight to further analyse the optimisation results. Optimal solution decisions under different thermodynamic weights are shown in Fig. 4(b). The effects of different thermodynamic weights and distribution pressures on energy efficiency and EPC are shown in Fig. 5(a) and (b), respectively. The maximum energy efficiency increases with the decrease in the distribution pressure. Under each distribution pressure, the system attains its maximum energy efficiency when the thermodynamic weight is 1. The maximum energy efficiency of 32.78% with the EPC of 0.013 $ kWh^{-1} is achieved when the thermodynamic weight is 1 and the distribution pressure is 1 MPa. Although both energy efficiency and EPC increase as the thermodynamic weight increases, their trends are different. As the thermodynamic weight increases, the energy efficiency increases approximately linearly. This is particularly noticeable when the thermodynamic weight is greater than 0.3. However, the EPC initially experiences a moderate increase as the thermodynamic weight increases. Subsequently, its growth rate gradually intensifies. This pattern becomes more evident with higher distribution pressure, which indicates a higher economic cost.

3.1.2. Optimum effectiveness

The optimisation results in the form of effectiveness are shown in Fig. 6(a), where different colours and markers represent different effectiveness values. The ideal point at each distribution pressure is marked with a red circle. At distribution pressures of 1 MPa or 4 MPa, higher effectiveness is linked to higher energy efficiency. However, at a distribution pressure of 7 MPa, the average effectiveness is significantly lower compared to 1 MPa and 4 MPa. The optimal effectiveness situation at different thermodynamic weights under three distribution pressures is shown in Fig. 6(b). The effectiveness of 0, corresponding to the basic ORC configuration, is preferred when the thermodynamic weight is low, indicating that there is a greater emphasis on the economic metric, whereas the effectiveness greater than 0, corresponding to the recuperative ORC configuration, is preferred when the thermodynamic weight is high, indicating that there is a greater emphasis on the thermodynamic metric. Specifically, when the thermodynamic weight is less than 0.5, the effectiveness under all distribution pressures remains at 0, indicating that the basic ORC is the optimum configuration. As the thermodynamic weight increases, the effectiveness increases to greater than 0 indicating that the recuperative ORC is the optimum configuration. At distribution pressures of 1 MPa and 4 MPa, the maximum effectiveness occurs when the thermodynamic weight reaches 1, with only a minor difference between them. However, when the distribution pressure is 7 MPa, the effectiveness decreases as the thermodynamic weight approaches 1.

3.1.3. Optimum working fluid

The optimisation results in the form of the working fluid under three distribution pressures are shown in Fig. 7, where the different working fluids are represented in different colours and markers. The ideal point at each distribution pressure is marked with a red circle. Although a total of 11 working fluid candidates are included during optimisation, only four of them are shown in the optimisation results. For distribution pressures of 1 MPa and 4 MPa, their Pareto frontiers comprise the same working fluid of isobutane, propane, and propylene. However, the disparity lies in the positioning of isobutane. Specifically, isobutane is the optimum working fluid in the region of higher energy efficiency and EPC when the distribution pressure is 4 MPa, whereas isobutane occupies the region of lower energy efficiency and EPC when the distribution pressure is 1 MPa. For a distribution pressure of 7 MPa, the Pareto frontier comprises four working substances, with the addition of R1234yf.

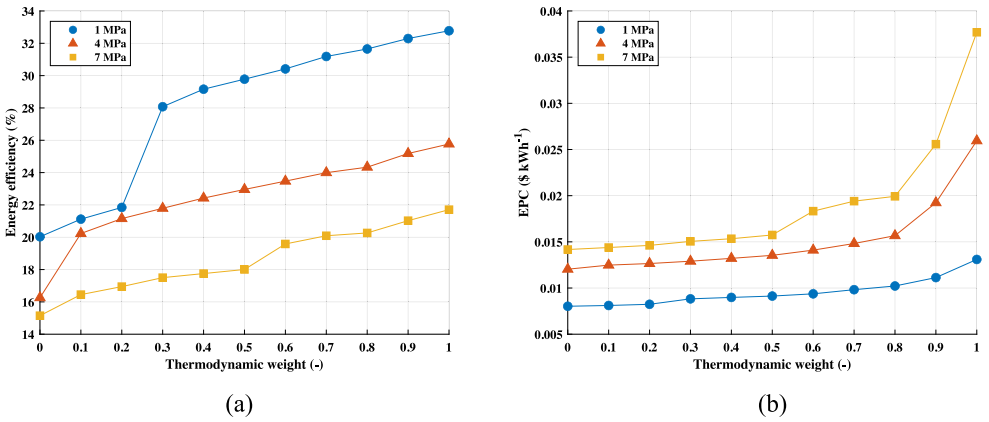

Fig. 5. The optimum objective ((a) Energy efficiency; (b) EPC) of different thermodynamic weights from 0 to 1 under three distribution pressures 1 MPa, 4 MPa and 7 MPa.

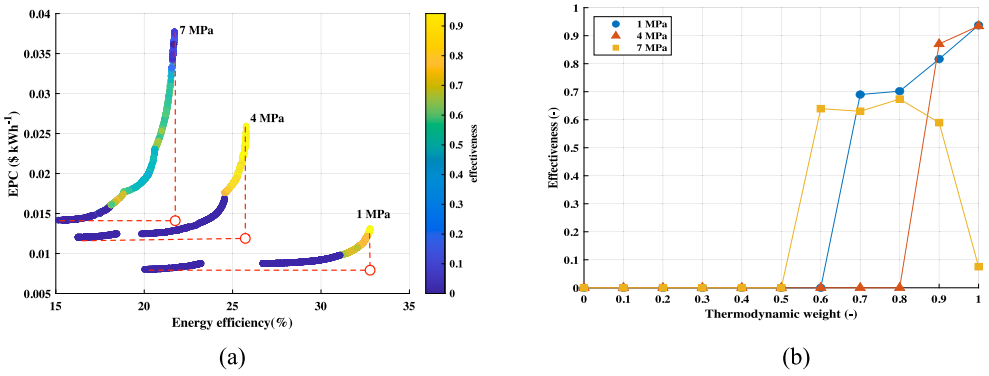

Fig. 6. (a) The optimisation results under three distribution pressures in the form of effectiveness; (b) The optimum effectiveness under three distribution pressures at different thermodynamic weights.

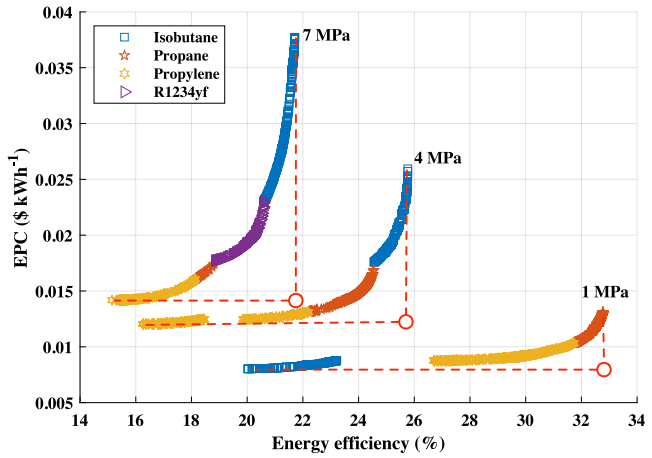

Fig. 7. The optimisation results in the form of working fluid under three distribution pressures 1 MPa, 4 MPa and 7 MPa.

Table 9 lists the optimum working fluids at different thermodynamic weights under three distribution pressures. In most weight scenarios, Propylene and Propane stand out as optimal working fluids. Although propylene emerges as the optimal working fluid in all three distribution pressure conditions when the thermodynamic weight is 0.3, the optimum working fluids in the three distribution pressures are not always the same. When the distribution pressure is 4 MPa, the optimal working fluids change from Propylene to Propane and finally to isobutane as the thermodynamic weight increases. Whereas when the distribution pressure is 7 MPa, propylene and R1234yf replace propane within the thermodynamic weight intervals of 0.4 to 0.5 and 0.6 to 0.8, respectively. When the distribution pressure is 1 MPa, although the types of optimal working fluids are the same as when the distribution pressure is 4 MPa, their order is reversed. As the thermodynamic weight increases, the optimal working fluids are isobutane, propylene, and propane, respectively.

3.2. Optimum results comparison

Two typical conditions are presented and compared: the balanced case (W_1 = 0.5) where thermodynamic and economic performance are treated equally and the maximum case (W_1 = 1) where only thermodynamic performance is considered, denoted in Fig. 8. The two cases are compared in terms of optimum parameters and optimum objectives.

3.2.1. Optimum parameter comparison

The optimum configurations and T-s diagrams of the balanced case (W_1 = 0.5) under the distribution pressures 1 MPa, 4 MPa, and 7 MPa are shown in Fig. 9, respectively.

Table 9
The optimum working fluids at different distribution pressures under various thermodynamic weights.

P_{dis} \ W_1	0	0.1	0.2	0.3	0.4	0.5	0.6	0.7	0.8	0.9	1
1 MPa	Isobutane	Isobutane	Isobutane	Propylene	Propylene	Propylene	Propylene	Propylene	Propylene	Propane	Propane
4 MPa	Propylene	Propylene	Propylene	Propylene	Propane	Propane	Propane	Propane	Propane	Isobutane	Isobutane
7 MPa	Propylene	Propylene	Propylene	Propylene	Propylene	Propylene	R1234yf	R1234yf	R1234yf	Isobutane	Isobutane

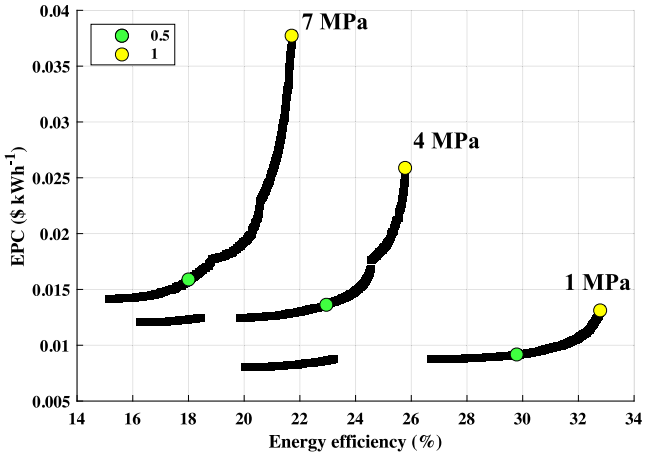

Fig. 8. Two typical conditions: the balanced case (W_1 = 0.5) and the maximum case (W_1 = 1) under three distribution pressures 1 MPa, 4 MPa and 7 MP.

For three distribution pressures, the optimal configurations exhibit substantial similarities. For example, all optimal ORC systems are basic ORC configurations. Moreover, the condensation temperature consistently reaches the lower boundary of the normal boiling point temperature (NBPT), although the optimal working fluid varies under different distribution pressures. However, the optimal configurations of their DEC subsystems are different. For example, when the distribution pressure reaches 1 MPa, both the TUR2 NG turbine and the AUX2 auxiliary heat exchanger are incorporated into the system, serving to raise the LNG temperature to the target distribution temperature after expansion. At a distribution pressure of 4 MPa, the LNG cycle only employs a TUR2 NG turbine to maximise the power output derived from natural gas expansion. When the distribution pressure is 7 MPa, neither the NG turbine nor the auxiliary heat exchanger is needed, and the LNG is heated to the distribution temperature by the ORC working fluid and the geothermal heat sources in CON and AUX1, respectively. This is because the benefit of NG expansion diminishes as the distribution pressure increases. Moreover, although this configuration suffers from the absence of natural gas expansion work, it also reduces the capital investment in the turbine, thus reaching the trade-off between thermodynamic performance and economic considerations.

The optimum configurations and T-s diagrams of the maximum case (W_1 = 1) under the distribution pressures 1 MPa, 4 MPa and 7 MPa are shown in Fig. 10, respectively. Regarding the system configuration, all optimal ORC configurations adopt the recuperative ORC, and the NG turbine is included in all DEC subsystems. The difference lies in whether the AUX2 auxiliary heat exchanger is included. The LNG regasification pressure and NG temperature at the turbine outlet increase in parallel with the increase in distribution pressure. Hence, under the conditions of 1 MPa and 4 MPa, the NG temperature at the turbine outlet is low, requiring an auxiliary heat exchanger AUX2 to heat the NG back to the distribution temperature. However, as the distribution pressure increases to 7 MPa, the NG temperature at the turbine outlet already meets the distribution temperature requirement, thus eliminating the need for the AUX2 auxiliary heat exchanger for additional heating. In terms of the pinch-point temperature difference (PPTD), the PPTD position in the evaporator is consistently observed at the turbine inlet, while in the condenser, the PPTD position is uniformly observed at the exit of the subcooling section. Moreover, the inlet temperature of the turbine consistently reaches its upper limit, which entails the smallest PPTD and helps to achieve a higher energy efficiency. For the same reason, the condensation temperature consistently reaches the lower boundary of the NBPT for each working fluid, although the optimal working fluid varies under different distribution pressures. In addition, the PPTDs in the balanced case are much larger than those in the maximum case.

3.2.2. Optimum objective comparison

The optimum objectives comparison between the balanced case (W_1 = 0.5) and the maximum case (W_1 = 1) under three distribution pressures of 1 MPa, 4 MPa, and 7 MPa is shown in Fig. 11.

In both the balanced and maximum cases, an increase in the distribution pressure results in a corresponding decline in energy efficiency and an increase in EPC. Hence, at the distribution pressure of 1 MPa, the maximum case can produce the maximum energy efficiency of 32.78% with the EPC of 0.013 \$ kWh^{-1}. Although the balanced case can achieve the minimum EPC of 0.009 \$ kWh^{-1} with an energy efficiency of 29.78%. Although both energy efficiency and EPC in the maximum case exceed those in the balanced case, the degrees of difference vary. The energy efficiency of the balanced case is nearly commensurate with that of the maximum case, yet its EPC is substantially lower. For example, when the distribution pressure is 7 MPa, the maximum case can achieve an energy efficiency of 21.71% with an EPC of 0.038 \$ kWh^{-1}, while the balanced case can achieve the energy efficiency of 18.00% with only the EPC of 0.016 \$ kWh^{-1}. The balanced case can achieve an energy efficiency of 82.94% compared to that of the maximum case, which requires only 44.17% EPC. This is because the maximum case focusses solely on energy efficiency, while the balanced case considers both energy efficiency and economic metric EPC. Moreover, this advantage becomes more pronounced as the distribution pressure increases. For ORC systems, the single-objective optimisation in this study corresponds to the maximum case, focussing exclusively on achieving the highest thermodynamic efficiency. Conversely, the two-objective optimisation corresponds to the balanced case, considering both thermodynamic performance and economics equally. The comparison reveals that two-objective optimisation yields more holistic outcomes, balancing critical factors such as capital expenditure and operational costs relevant to practical applications. For example, a slight reduction in thermodynamic efficiency could significantly reduce equipment costs, ultimately enhancing overall profitability. This highlights how minor thermodynamic compromises can generate notable economic benefits, positioning two-objective optimisation as a more practical method for real-world decision making.

4. Conclusion

Within the realm of ORC-LNG optimisation challenges, the determination of optimal parameters, working fluids, and system configurations play pivotal roles. In addition, these factors are closely related

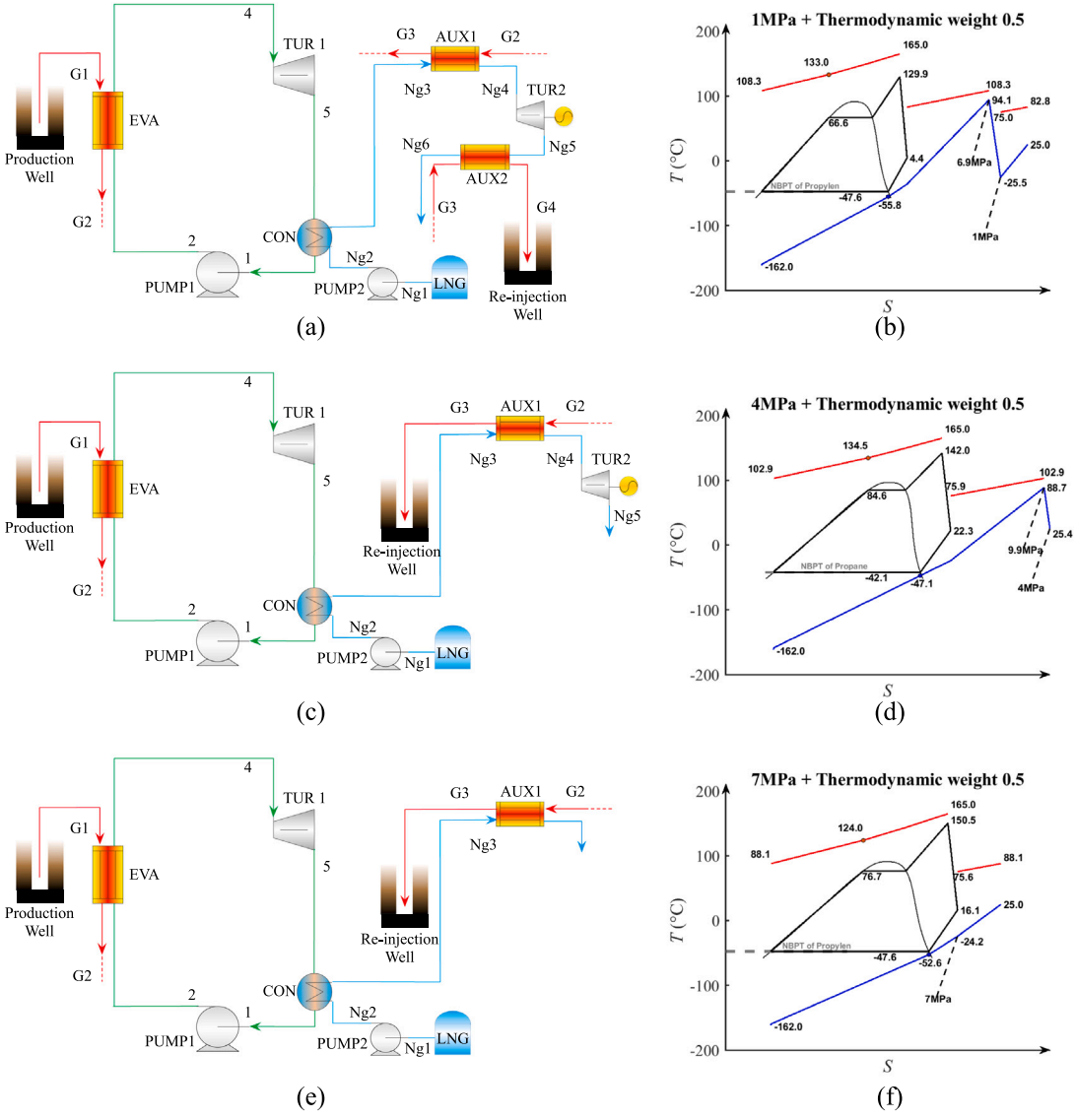

Fig. 9. The optimum configurations and T-s diagrams of the balanced case under three distribution pressures ((a), (b) 1 MPa; (c), (d) 4 MPa; (e), (f) 7 MPa).

to the operational requirements of the NG, such as the requirement of the NG distribution pressure. Hence, in this paper, the combined ORC system utilising both the cryogenic energy from LNG and the renewable thermal energy from geothermal is constructed and optimised at different natural gas distribution pressures. Eight operational parameters are optimised with the objective of maximising energy efficiency and minimising EPC. 11 commonly used working fluids are selected and up to 16 different combined ORC configurations are included during the optimisation process. Moreover, this study addresses the selection of optimal integrated ORC configurations within one optimisation. This methodology markedly boosts the efficiency of the optimisation. The principal findings can be summarised as follows.

(1) The multi-objective multi-fluid multi-configuration optimisation is capable of providing a comprehensive result to guide the selection of operational parameters, working fluids, and system configurations. In addition, the novel method of including different configurations within each optimisation process can significantly reduce the number of required optimisations and diminish the total optimisation time. The computational time for the combined ORC system at each distribution pressure is approximately 5 h.

(2) The optimisation result shows that although energy efficiency is positively correlated with EPC under each distribution pressure, the extent varies in relation to distribution pressure. As the distribution pressure decreases, the extent to which the EPC increases with energy efficiency decreases progressively, and the system can achieve a higher maximal energy efficiency while also reducing the minimum EPC. The maximum energy efficiency of 32.78% can be achieved with an EPC of 0.013 $ kWh^{-1} when the distribution pressure is 1 MPa.

(3) The recuperative ORC is preferred when the thermodynamic metric is emphasised, while the basic ORC is preferred when the economic metric dominates at distribution pressures of 1 MPa and 4 MPa. However, this is not the case at 7 MPa. For the maximum case, the optimal pinch-point temperature differences of both the evaporator and the condenser reach their lower limits, while those in the balanced case are significantly larger.

(4) Although the maximum case can achieve the optimal thermodynamic performance, it is concurrently associated with worse

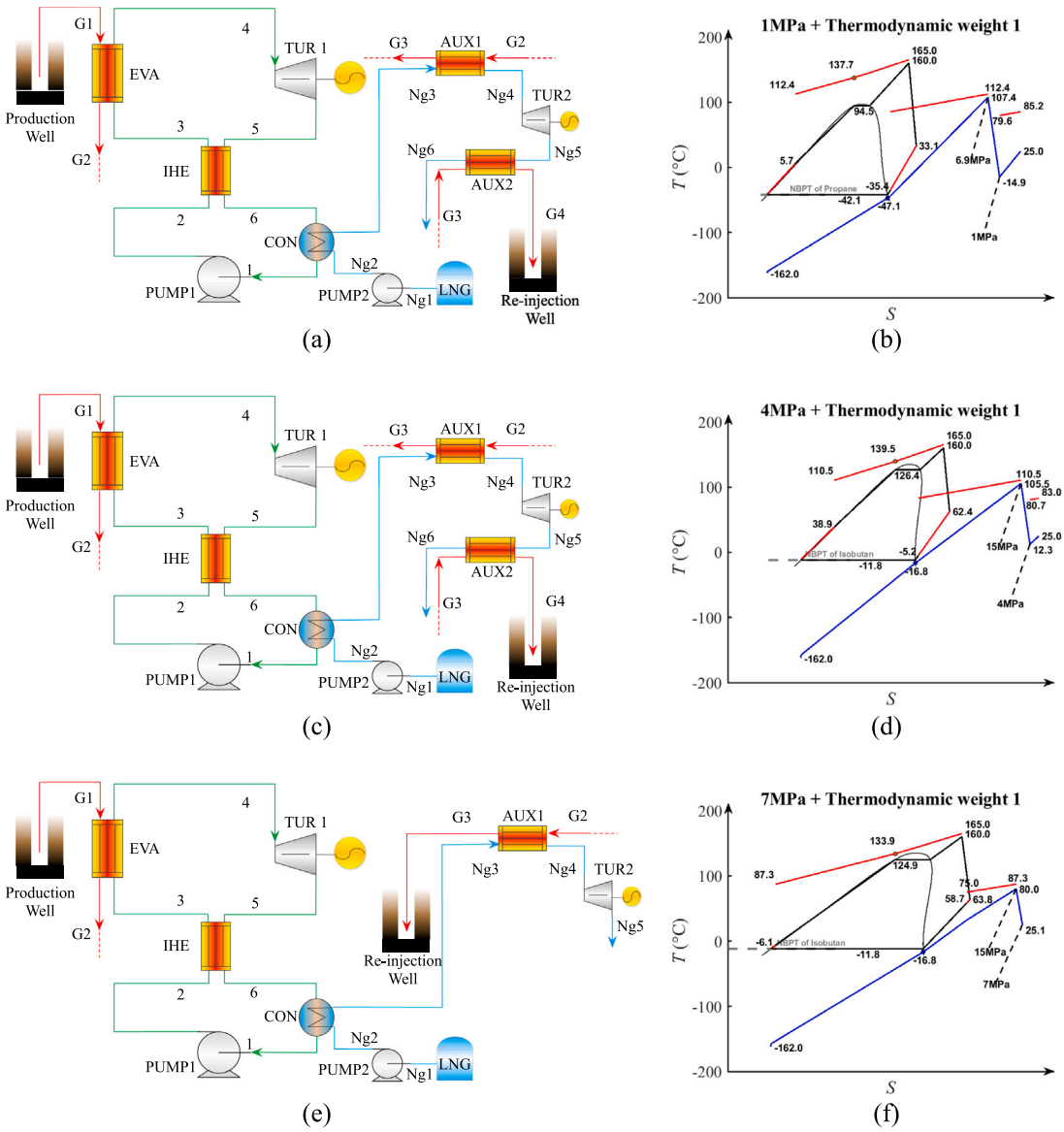

Fig. 10. The optimum configurations and T-s diagrams of the maximum case under three distribution pressures ((a), (b) 1 MPa; (c), (d) 4 MPa; (e), (f) 7 MPa).

economic performance. The balanced case achieves an energy efficiency of 82.94% with only 44.17% EPC compared to the maximum case at a distribution pressure of 7 MPa, offering significant economic benefits with minimal thermodynamic losses.

CRediT authorship contribution statement

Han Zhang: Writing – review & editing, Writing – original draft, Methodology, Investigation, Formal analysis, Data curation, Conceptualization. **Giovanna Cavazzini:** Writing – review & editing, Methodology, Investigation, Formal analysis, Data curation, Conceptualization. **Giacomo Zanetti:** Writing – review & editing, Methodology, Investigation, Formal analysis, Data curation, Conceptualization. **Alberto Benato:** Writing – review & editing, Writing – original draft, Methodology, Investigation, Formal analysis, Data curation, Conceptualization.

Declaration of competing interest

The authors declare that they have no known competing financial interests or personal relationships that could have appeared to influence the work reported in this paper.

Appendix A. Optimum optimisation objectives of different thermodynamic weight (W_1) under three distribution pressures

See Tables A.10 and A.11.

Appendix B. Optimum parameters of different thermodynamic weight (W_1) under three distribution pressures

See Tables B.12–B.19.

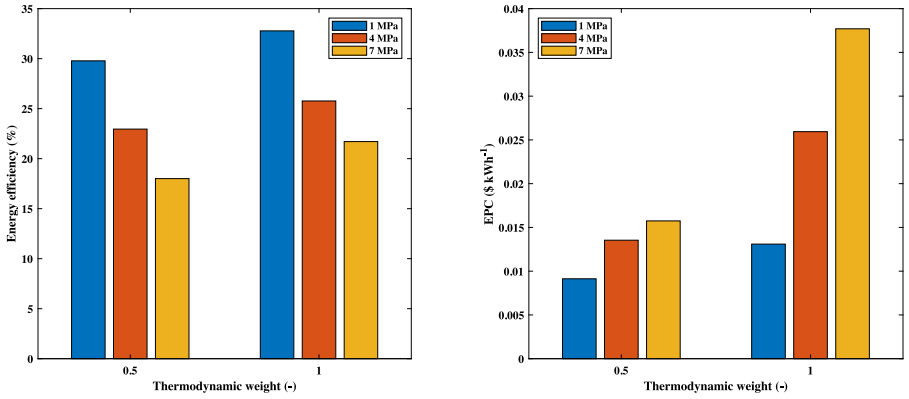

(a) (b)

Fig. 11. The optimum objective ((a) energy efficiency; (b) EPC) comparison under the balanced case (W_1 = 0.5) and the maximum case (W_1 = 1) under three distribution pressures 1 MPa, 4 MPa, and 7 MPa.

Table A.10
Optimisation result of system efficiency.

P_{dis} \ W_1	0	0.1	0.2	0.3	0.4	0.5	0.6	0.7	0.8	0.9	1
1 MPa	20.0288	21.1187	21.8452	28.0765	29.1603	29.7797	30.4149	31.1854	31.6498	32.2960	32.7763
4 MPa	16.2583	20.2316	21.1529	21.7905	22.4228	22.9559	23.4708	23.9953	24.3348	25.1807	25.7683
7 MPa	15.1463	16.4504	16.9447	17.4999	17.7516	18.0045	19.5849	20.0921	20.2662	21.0248	21.7067

Table A.11
Optimisation result of EPC.

P_{dis} \ W_1	0	0.1	0.2	0.3	0.4	0.5	0.6	0.7	0.8	0.9	1
1 MPa	0.0080	0.0081	0.0082	0.0088	0.0090	0.0091	0.0094	0.0098	0.0102	0.0111	0.0131
4 MPa	0.0120	0.0125	0.0127	0.0129	0.0132	0.0135	0.0141	0.0148	0.0157	0.0192	0.0259
7 MPa	0.0142	0.0144	0.0146	0.0151	0.0153	0.0157	0.0183	0.0194	0.0199	0.0256	0.0377

Table B.12
Optimisation result of effectiveness.

P_{dis} \ W_1	0	0.1	0.2	0.3	0.4	0.5	0.6	0.7	0.8	0.9	1
1 MPa	0	0	0	0	0	0	0	0.6899	0.7019	0.8167	0.9371
4 MPa	0	0	0	0	0	0	0	0	0	0.8704	0.9344
7 MPa	0	0	0	0	0	0	0.6395	0.6302	0.6738	0.5896	0.0753

Table B.13
Optimisation result of LNG regasification pressure.

P_{dis} \ W_1	0	0.1	0.2	0.3	0.4	0.5	0.6	0.7	0.8	0.9	1
1 MPa	8.0598	9.5706	10.9523	6.5950	6.7211	6.9223	6.8484	6.5731	6.6644	7.0092	6.9433
4 MPa	4.0000	7.5250	8.5722	10.0700	9.8883	9.8900	15.0000	15.0000	15.0000	15.0000	15.0000
7 MPa	7.0000	7.0000	7.0000	7.0117	7.0032	7.0053	15.0000	15.0000	15.0000	15.0000	15.0000

Table B.14
Optimisation result of evaporation temperature.

P_{dis} \ W_1	0	0.1	0.2	0.3	0.4	0.5	0.6	0.7	0.8	0.9	1
1 MPa	−6.7486	−6.7489	−6.7490	59.0921	64.0606	66.5653	70.4659	75.9682	77.1954	84.1009	94.5078
4 MPa	59.4451	62.1680	66.0391	72.0234	83.0040	84.5552	86.8783	89.9850	91.0299	113.0759	126.4154
7 MPa	62.5391	67.1294	72.7666	75.4794	74.2848	76.7243	91.5345	92.7167	92.7321	116.1001	124.8802

Table B.15
Optimisation result of condensation temperature.

P_{dis} \ W_1	0	0.1	0.2	0.3	0.4	0.5	0.6	0.7	0.8	0.9	1
1 MPa	−11.7490	−11.7490	−11.7490	−47.6192	−47.6167	−47.6176	−47.6178	−47.5629	−47.6192	−42.1138	−42.0836
4 MPa	−47.6190	−47.6170	−47.4672	−47.5468	−42.0628	−42.1124	−42.0588	−42.0654	−42.0748	−11.7490	−11.7490
7 MPa	−47.6192	−47.6192	−47.6191	−47.6191	−47.6191	−47.6191	−29.4851	−29.4851	−29.4851	−11.7490	−11.7488

Table B.16
Optimisation result of working fluid turbine inlet temperature.

P_{dis} \ W_1	0	0.1	0.2	0.3	0.4	0.5	0.6	0.7	0.8	0.9	1
1 MPa	−6.7486	−6.7488	−5.8382	115.8082	123.3557	129.9335	136.7581	143.8380	150.2411	153.8391	159.9808
4 MPa	114.9456	125.7565	133.9567	138.4210	134.3743	141.9830	146.1516	152.0982	156.4759	153.9018	159.9850
7 MPa	124.1202	134.5835	138.9532	144.4046	147.8416	150.5160	140.9712	149.9529	152.0975	154.1230	159.9992

Table B.17
Optimisation result of NG turbine inlet temperature.

P_{dis} \ W_1	0	0.1	0.2	0.3	0.4	0.5	0.6	0.7	0.8	0.9	1
1 MPa	124.4814	130.1994	133.9678	87.9164	93.8244	94.1267	97.0850	100.1553	103.1155	105.5050	107.3277
4 MPa	126.7469	68.4374	77.9566	90.0874	88.2840	88.6856	98.3904	104.4736	108.6290	112.4516	105.4771
7 MPa	−38.8587	−30.6636	−29.9270	−27.7180	−24.4706	−24.1938	80.9041	80.2481	80.0874	80.0575	80.0192

Table B.18
Optimisation result of evaporator PPTD.

P_{dis} \ W_1	0	0.1	0.2	0.3	0.4	0.5	0.6	0.7	0.8	0.9	1
1 MPa	169.4463	169.0647	169.2142	74.6571	69.5655	66.4224	62.5249	57.3285	55.5254	48.4117	43.1767
4 MPa	62.2472	65.7612	64.2809	62.6964	52.8373	49.9880	52.1425	50.6698	50.0556	24.9848	13.0518
7 MPa	60.7242	55.4650	52.7270	49.1366	48.9940	47.2455	44.8213	42.5367	41.2123	16.7587	9.0351

Table B.19
Optimisation result of condenser PPTD.

P_{dis} \ W_1	0	0.1	0.2	0.3	0.4	0.5	0.6	0.7	0.8	0.9	1
1 MPa	139.1765	137.0112	137.9365	46.2552	42.1551	40.5157	39.6918	17.2132	17.6363	13.8318	8.6864
4 MPa	38.7205	43.6149	46.8833	47.4515	43.3255	46.4771	50.4202	52.4626	54.8304	10.2441	7.8925
7 MPa	41.1481	39.3859	37.7807	38.6639	40.1493	40.3410	20.1650	22.2644	20.9382	17.9826	26.3073

Data availability

The data that has been used is confidential.

References

[1] Lecompte S, Huisseune H, van den Broek M, Vanslambrouck B, De Paepe M. Review of organic rankine cycle (ORC) architectures for waste heat recovery. Renew Sustain Energy Rev 2015;47:448–61.

[2] Saleh B, Koglbauer G, Wendland M, Fischer J. Working fluids for low-temperature organic rankine cycles. Energy 2007;32(7):1210–21.

[3] Hung T-C. Waste heat recovery of organic rankine cycle using dry fluids. Energy Convers Manage 2001;42(5):539–53.

[4] Li W, Feng X, Yu LJ, Xu J. Effects of evaporating temperature and internal heat exchanger on organic rankine cycle. In: SET 2010 special issue, Appl Therm Eng In: SET 2010 special issue, 2011;31(17).4014–23,

[5] Pezzuolo A, Benato A, Stoppato A, Mirandola A. The ORC-PD: A versatile tool for fluid selection and organic rankine cycle unit design. Energy 2016;102:605–20.

[6] Redjeb Y, Kaabeche-Djerafi K, Stoppato A, Benato A. The IRC-PD tool: A code to design steam and organic waste heat recovery units. Energies 2021;14(18):5611.

[7] Stoppato A, Benato A. Life cycle assessment of a commercially available organic rankine cycle unit coupled with a biomass boiler. Energies 2020;13(7):1835.

[8] Cavazzini G, Giacomel F, Benato A, Nascimben F, Ardizzon G. Analysis of the inner fluid-dynamics of scroll compressors and comparison between CFD numerical and modelling approaches. Energies 2021;14(4):1158.

[9] Weitzer M, Müller D, Karl J. Two-phase expansion processes in heat pump–ORC systems (carnot batteries) with volumetric machines for enhanced off-design efficiency. Renew Energy 2022;199:720–32.

[10] Lin W, Huang M, Gu A. A seawater freeze desalination prototype system utilizing LNG cold energy. In: Special issue on the 5th international conference on energy engineering and environmental engineering (ICEEEE2017), 15-16 April 2017, xiamen, China, Int J Hydrog Energy In: Special issue on the 5th international conference on energy engineering and environmental engineering (ICEEEE2017), 15-16 April 2017, xiamen, China, 2017;42(29).18691–8,

[11] Sun Z. Thermodynamic optimization and comparative study of different orc configurations utilizing the exergies of LNG and low grade heat of different temperatures. Energy 2018;13.

[12] Zhang H-H, Li M-J, Feng Y-Q, Xi H, Hung T-C. Assessment and working fluid comparison of steam rankine cycle-organic rankine cycle combined system for severe cold territories. Case Stud Therm Eng 2021;28:101601.

[13] He T, Lv H, Shao Z, Zhang J, Xing X, Ma H. Cascade utilization of LNG cold energy by integrating cryogenic energy storage, organic rankine cycle and direct cooling. Appl Energy 2020;277:115570.

[14] Domingues A, Matos HA, Pereira PM. Novel integrated system of LNG regasification/electricity generation based on a cascaded two-stage rankine cycle, with ternary mixtures as working fluids and seawater as hot utility. Energy 2022;238:121972.

[15] Choi HW, Na S-I, Hong SB, Chung Y, Kim DK, Kim MS. Optimal design of organic rankine cycle recovering LNG cold energy with finite heat exchanger size. Energy 2021;217:119268.

[16] Zhang M-G, Zhao L-J, Liu C, Cai Y-L, Xie X-M. A combined system utilizing LNG and low-temperature waste heat energy. Appl Therm Eng 2016;101:525–36.

[17] Wei D, Lu X, Lu Z, Gu J. Performance analysis and optimization of organic rankine cycle (ORC) for waste heat recovery. Energy Convers Manage 2007;48(4):1113–9.

[18] Emadi MA, Mahmoudimehr J. Modeling and thermo-economic optimization of a new multi-generation system with geothermal heat source and LNG heat sink. Energy Convers Manage 2019;189:153–66.

[19] Sun Z. Optimizations and comparison of three two-stage rankine cycles under different heat source temperatures and NG distribution pressures. Energy Convers Manage 2020;17.

[20] Yari M. Exergetic analysis of various types of geothermal power plants. Renew Energy 2010;35(1):112–21.

[21] Mosaffa AH, Mokarram NH, Farshi LG. Thermo-economic analysis of combined different ORCs geothermal power plants and LNG cold energy. Geothermics 2017;65:113–25.

[22] Ghaebi H, Parikhani T, Rostamzadeh H. A novel trigeneration system using geothermal heat source and liquefied natural gas cold energy recovery: Energy, exergy and exergoeconomic analysis. Renew Energy 2018;119:513–27.

[23] Emadi MA, Pourrahmani H, Moghimi M. Performance evaluation of an integrated hydrogen production system with LNG cold energy utilization. Int J Hydrog Energy 2018;43(49):22075–87.
[24] Parikhani T, Gholizadeh T, Ghaebi H, Sadat SMS, Sarabi M. Exergoeconomic optimization of a novel multigeneration system driven by geothermal heat source and liquefied natural gas cold energy recovery. J Clean Prod 2019;209:550–71.
[25] Dai Y, Wang J, Gao L. Parametric optimization and comparative study of organic rankine cycle (ORC) for low grade waste heat recovery. Energy Convers Manage 2009;50(3):576–82.
[26] Roy JP, Mishra MK, Misra A. Parametric optimization and performance analysis of a waste heat recovery system using organic rankine cycle. In: The 3rd international conference on sustainable energy and environmental protection, SEEP 2009, Energy In: The 3rd international conference on sustainable energy and environmental protection, SEEP 2009, 2010;35(12).5049–62,
[27] Vaja I, Gambarotta A. Internal combustion engine (ICE) bottoming with organic rankine cycles (ORCs). In: ECOS 2008, Energy In: ECOS 2008, 2010;35(2).1084–93,
[28] Nguyen TQ, Slawnwhite JD, Boulama KG. Power generation from residual industrial heat. Energy Convers Manage 2010;51(11):2220–9.
[29] Siddiqi MA, Atakan B. Alkanes as fluids in rankine cycles in comparison to water, benzene and toluene. In: The 24th international conference on efficiency, cost, optimization, simulation and environmental impact of energy, ECOS 2011, Energy In: The 24th international conference on efficiency, cost, optimization, simulation and environmental impact of energy, ECOS 2011, 2012;45(1).256–63,
[30] Mago PJ, Chamra LM, Srinivasan K, Somayaji C. An examination of regenerative organic rankine cycles using dry fluids. Appl Therm Eng 2008;28(8–9):998–1007.
[31] Sun Z, Wang J, Dai Y, Wang J. Exergy analysis and optimization of a hydrogen production process by a solar-liquefied natural gas hybrid driven transcritical CO2 power cycle. Int J Hydrog Energy 2012;37(24):18731–9.
[32] Han F, Wang Z, Ji Y, Li W, Sundén B. Energy analysis and multi-objective optimization of waste heat and cold energy recovery process in LNG-fueled vessels based on a triple organic rankine cycle. Energy Convers Manage 2019;195:561–72.
[33] Badami M, Bruno JC, Coronas A, Fambri G. Analysis of different combined cycles and working fluids for LNG exergy recovery during regasification. Energy 2018;159:373–84.
[34] Ferreira P, Catarino I, Vaz D. Thermodynamic analysis for working fluids comparison in rankine-type cycles exploiting the cryogenic exergy in liquefied natural gas (LNG) regasification. Appl Therm Eng 2017;121:887–96.
[35] Mehrenjani JR, Gharehghani A, Sangesaraki AG. Machine learning optimization of a novel geothermal driven system with LNG heat sink for hydrogen production and liquefaction. Energy Convers Manage 2022;254:115266.
[36] Sadreddini A, Ashjari MA, Fani M, Mohammadi A. Thermodynamic analysis of a new cascade ORC and transcritical CO2 cycle to recover energy from medium temperature heat source and liquefied natural gas. Energy Convers Manage 2018;167:9–20.
[37] Pan J, Li M, Zhu M, Li R, Tang L, Bai J. Energy, exergy and economic analysis of different integrated systems for power generation using LNG cold energy and geothermal energy. Renew Energy 2023;202:1054–70.
[38] Sun Z, Zhao Q, Wu Z, Lin K. Thermodynamic comparison of modified rankine cycle configurations for LNG cold energy recovery under different working conditions. Energy Convers Manage 2021;239:114141.
[39] Turton R, Bailie RC, Whiting WB, Shaeiwitz JA. Analysis, synthesis and design of chemical processes. Pearson Education; 2008.
[40] Zhang H, Cavazzini G, Benato A. Multi-objective optimisation of ORC–LNG systems using the novel one-shot optimisation method. Energy 2024;313:133629.
[41] Wang L, Bu X, Li H. Multi-objective optimization and off-design evaluation of organic rankine cycle (ORC) for low-grade waste heat recovery. Energy 2020;203:117809.